Inorganic Chemistry

ARTICLE

pubs.acs.org/IC

Tunable Full-Color Emitting $BaMg_2Al_6Si_9O_{30}:Eu^{2+}$, Tb^{3+}, Mn^{2+} Phosphors Based on Energy Transfer

Wei Lü,[†,‡] Zhendong Hao,[†] Xia Zhang,[†] Yongshi Luo,[†] Xiaojun Wang,[†,§] and Jiahua Zhang*[,†]

[†]Key Laboratory of Excited State Processes, Changchun Institute of Optics, Fine Mechanics and Physics, Chinese Academy of Sciences, 16 Eastern South Lake Road, Changchun 130033, China

[‡]Graduate School of Chinese Academy of Sciences, Beijing, 100039, China

[§]Department of Physics, Georgia Southern University, Statesboro, Georgia 30460, United States

ABSTRACT: A series of single-phase full-color emitting $BaMg_2Al_6Si_9O_{30}:Eu^{2+}$, Tb^{3+}, Mn^{2+} phosphors has been synthesized by solid-state reaction. Energy transfer from Eu^{2+} to Tb^{3+} and Eu^{2+} to Mn^{2+} in $BaMg_2Al_6Si_9O_{30}$ host matrix is studied by luminescence spectra and energy-transfer efficiency and lifetimes. The wavelength-tunable white light can be realized by coupling the emission bands centered at 450, 542, and 610 nm ascribed to the contribution from Eu^{2+} and Tb^{3+} and Mn^{2+}, respectively. By properly tuning the relative composition of Tb^{3+}/Mn^{2+}, chromaticity coordinates of (0.31, 0.30), high color rendering index R_a = 90, and correlated color temperature (CCT) = 5374 K can be achieved upon excitation of UV light. Thermal quenching properties reveal that $BaMg_2Al_6Si_9O_{30}$: Eu^{2+}, Tb^{3+}, Mn^{2+} exhibits excellent characteristics even better than that of YAG:Ce. Our results indicate our white $BaMg_2Al_6Si_9O_{30}:Eu^{2+}$, Tb^{3+}, Mn^{2+} can serve as a key material for phosphor-converted light-emitting diode and fluorescent lamps.

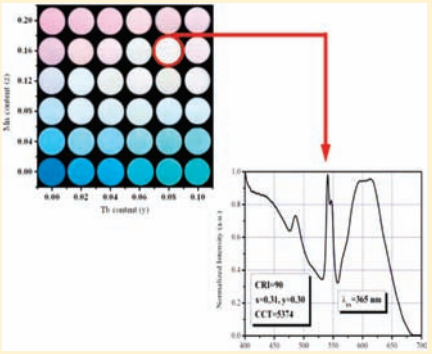

1. INTRODUCTION

As the two important lighting sources, fluorescent lamps (FLs) and light-emitting diode (LED) lamps have been developed for application in general lighting sources and components of backlight for liquid-crystal displays (LCDs). Both applications now suffer from problems, for example, fluorescent lamps containing a mixture of triphosphors, the blue-emitting $BaMgAl_{10}O_{17}:Eu^{2+}$, the red-emitting $Y_2O_3:Eu^{3+}$, and the green-emitting $LaPO_4:Ce^{3+}$, Tb^{3+}, easily lead to a decrease of device efficiency, owing to the reabsorption. As for LED, typical white LED lamps are based on a phosphor down conversion of blue InGaN LEDs by $Y_3Al_5O_{12}:Ce^{3+}$(YAG:Ce)-based yellow phosphors.[1,2] However, the device based on YAG:Ce^{3+} phosphor exhibits a poor color rendering index (CRI ≈ 70−80) and a high correlated color temperature (CCT ≈ 7750 K) because of lacking a red light contribution.[3−5] In order to improve the white light quality of white LEDs and obtain a higher CRI, a UV LED chip coated with three emitting blue, green, and red phosphors is introduced.[6−8] This approach provides white LEDs with excellent CRIs, but a similar drawback arises as in FLs, owing to the strong reabsorption of the blue light by the red and green phosphors.[9,10] In this regard, a single-phase full-color emitting phosphor, which can be avoided by using single emitting component phosphors with higher luminous efficiency and excellent CRI, is considered to be potentially useful because of small color aberration, high color rendering, and low cost.

One of the strategies for generating white light from single-composition phosphors is by codoping a sensitizer and an activator into a crystalline matrix, using the principle of energy transfer (ET) from sensitizer to activator, such as Eu^{2+}/Mn^{2+},[11−15] Ce^{3+}/Mn^{2+},[16−18] and Ce^{3+}/Tb^{3+}[19,20] in a proper single host lattice. Mn^{2+} doped luminescent materials have been known to show wide-ranging emission from 500 to 700 nm, which is strongly affected by the crystal field of the host materials.[21] Owing to the forbidden $^4T_1 \rightarrow {}^6A_1$ transition of Mn^{2+}, the emission intensity of Mn^{2+} singly doped phosphor is low. While Tb^{3+} could be also an ideal emitting activator for phosphors showing sharp lines at 488, 543, and 582 nm.[22] However, the Tb^{3+} ion has only weak absorption peaks at about 300−400 nm due to the 4f−4f absorption transitions. Thus, it is necessary to enhance the emission intensity of Mn^{2+} and Tb^{3+} doped materials by introducing an efficient sensitizer, well-known for Eu^{2+}, that would possibly overcome all the drawbacks mentioned above.

In this research, we report our recent investigation results on the luminescence and color tunability of a full-color emitting BMAS:Eu^{2+}, Tb^{3+}, Mn^{2+} phosphor. By varying the relative dopant concentrations of Tb^{3+} and Mn^{2+}, white light can be generated with higher CRI and higher color stability. Energy transfer from Eu^{2+} to Tb^{3+} and Eu^{2+} to Mn^{2+} is investigated.

2. EXPERIMENTAL SECTION

2.1. Sample Preparation. The $Ba_{1-x}Mg_{2-y-z}Al_6Si_9O_{30}$ (BMAS): xEu^{2+}, yTb^{3+}, zMn^{2+} phosphors were synthesized by a high-temperature solid-state reaction. The constituent oxides or carbonates

Received: May 16, 2011
Published: July 19, 2011

   dx.doi.org/10.1021/ic201033e | *Inorg. Chem.* 2011, 50, 7846–7851

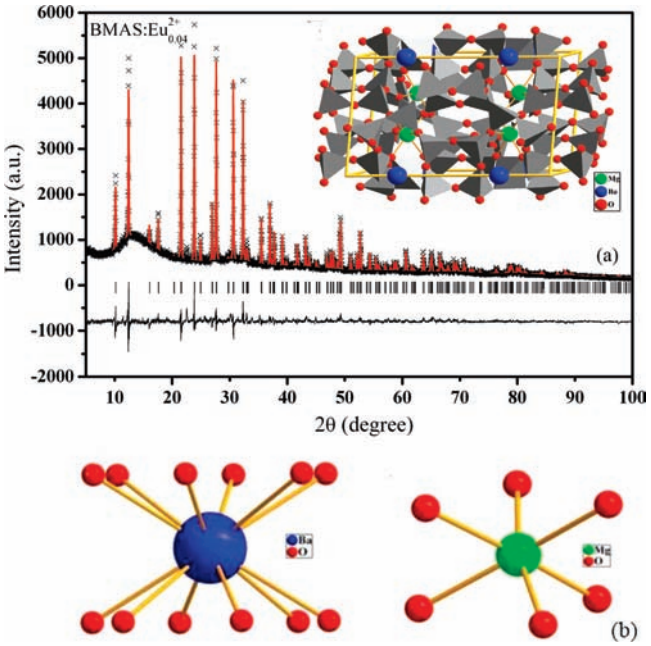

Figure 1. The experimental, calculated, and difference results of the XRD refinement of BMAS: Eu^{2+}.

$BaCO_3$ (99.9%), Al_2O_3 (99.9%), SiO_2 (99.9%), MgO(99.9%), Eu_2O_3 (99.99%), Tb_4O_7 (99.99%), and $MnCO_3$ (99.99%) were employed as the raw materials, which were mixed homogeneously by an agate mortar for 30 min, placed in a crucible with a lid, and then sintered in a tubular furnace at 1300 °C for 4 h in reductive atmosphere (10% H_2 + 90% N_2 mixed flowing gas).

2.2. Measurements and Characterization. The structure of sintered samples was identified by an X-ray powder diffractometer (Rigaku D/MAX-2500 V), using Cu Kα radiation (λ= 1.54056 Å). A step size of 0.02°(2θ) was used with a scanning speed of 4°/min. Crystal structure refinement employed the Rietveld method as implemented in the General Structure Analysis System (GSAS) program.[23] The measurements of photoluminescence (PL) and photoluminescence excitation (PLE) spectra were performed by using a Hitachi F4500 spectrometer equipped with a 150 W xenon lamp under a working voltage of 700 V. The excitation and emission slits were both set at 2.5 nm. The diffuse reflectance measurements are performed using the same spectrometer with $BaSO_4$ powder as a reflectance standard. In fluorescence lifetime measurements, the third harmonic (355 nm) of an Nd-doped yttrium aluminum garnet pulsed laser (Spectra- Physics, GCR 130) was used as an excitation source, and the signals were detected with a Tektronix digital oscilloscope (TDS 3052).

3. RESULTS AND DISCUSSION

3.1. Structural and Optical Properties of BMAS:Eu^{2+} Phosphor. Figure 1a shows the experimental, calculated, and difference results of the X-ray diffraction (XRD) refinement of BMAS: Eu^{2+}. The initial structural model was constructed with crystallographic data previously reported for BMAS (JCPDS 83−0740).[24] All of the observed XRD peaks are obtained with goodness of fit parameters R_{wp} = 8.42% and χ^2 = 2.846. BMAS: Eu^{2+} has a space group of *P6/mcc* with unit cell parameters $a = b$ = 10.1404 Å, and c = 14.3387 Å. Ba^{2+} and Mg^{2+} ions are tightly surrounded with tetrahedral SiO_4 and AlO_4 units. The oxygen atoms form bridges between SiO_4 and AlO_4 tetrahedral. There are two types of independent cation sites, namely, 12-fold coordinated

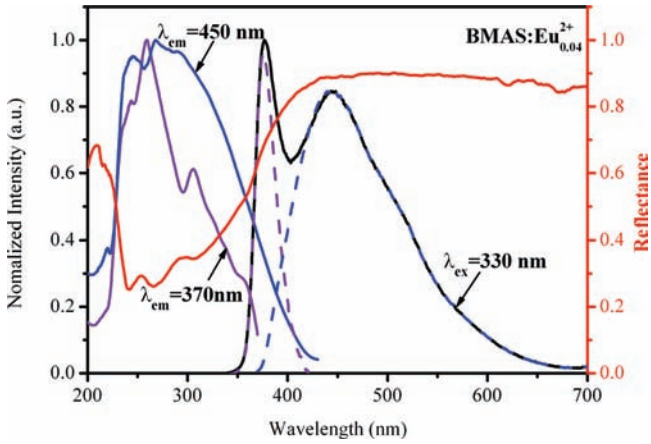

Figure 2. PLE, PL, and diffuse reflectance spectra of BMAS: Eu^{2+}.

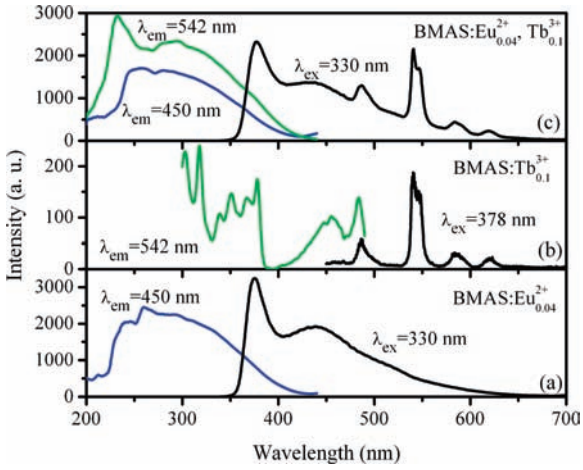

Figure 3. The excitation and emission spectra of BMAS: Eu^{2+} (a), BMAS: Tb^{3+} (b), and BMAS: Eu^{2+}, Tb^{3+}(c) phosphors.

Ba^{2+} and 6-fold coordinated Mg^{2+} sites, as presented in Figure 1b. When incorporated into the crystal structure of BMAS, Eu^{2+} may substitute for divalent cations, i.e., Ba^{2+} and Mg^{2+}. Their respective ionic radii with allowed oxygen-coordination number (CN) is 1.61 Å for Ba^{2+} with CN = 12, 0.72 Å for Mg^{2+} with CN = 6, 1.17 Å for Eu^{2+} with CN = 6, and 1.26 Å for Eu^{2+} with CN = 12. On the other hand, both $Tb^{3+}$and Mn^{2+}ions are expected to occupy Mg^{2+}sites because the ionic radii of Tb^{3+}(0.92 Å) and Mn^{2+}(0.66 Å) are close to that of Mg^{2+}(0.72 Å).

The PL, PLE, and diffuse reflectance spectra of BMAS: Eu^{2+} are depicted in Figure 2. The PL spectrum displays a broad band extending from 340 to 600 nm, which can be decomposed into two bands (dashed lines) centered at about 376 and 450 nm, respectively. The PLE spectra cover the UV spectral region of 200−400 nm, which is consistent with that observed in the reflection spectrum. However, the shape of the PLE spectrum monitored at 376 nm is remarkably different from that monitored at 450 nm. It is therefore speculated that the two emission bands are originated from $4f^65d^1-4f^7$ transition of Eu^{2+} ions occupying two different cation sites. In BMAS: Eu^{2+}, the average interatomic length between Eu^{2+} and oxygen (d_{Eu-O}) is 3.111 Å for Eu^{2+} occupying Ba^{2+} site and 2.138 Å for occupying Mg^{2+}site. In general, the bond length affects the crystal field strength

dx.doi.org/10.1021/ic201033e |*Inorg. Chem.* 2011, 50, 7846–7851

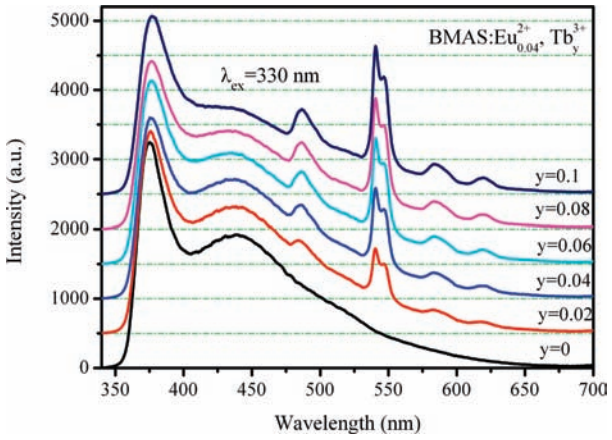

Figure 4. A series of the emission spectra for BMAS: 0.04Eu^{2+}, yTb^{3+} (y = 0, 0.02, 0.04, 0.06, 0.08, and 0.1) under excitation wavelength of 330 nm.

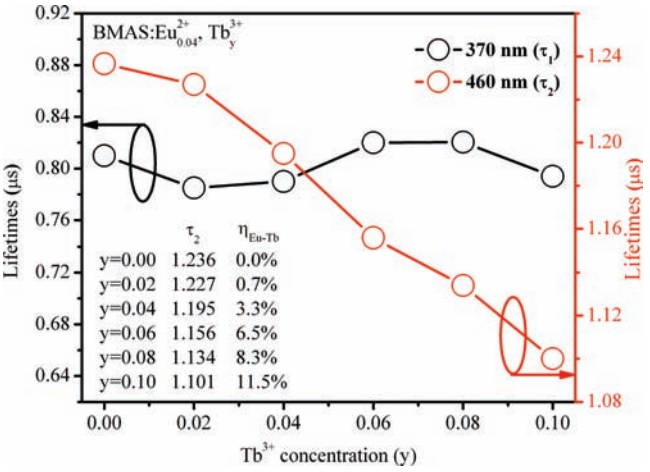

Figure 5. The lifetimes of Eu^{2+}(I) (τ_1) and Eu^{2+}(II) (τ_2) with different Tb^{3+}concentration.

significantly. Thus, we infer that the band at 376 nm is assigned to Eu^{2+}(I) occupying Ba^{2+} with a weak crystal field, and the other one at 450 nm corresponds to Eu^{2+}(II) occupying Mg^{2+} with a strong crystal field. In addition, the shape and the position of the band at 376 nm are in agreement with that in $BaSi_2Al_2O_8$:Eu^{2+}, which has the similar coordination environments around Eu^{2+} with the present BMAS: Eu^{2+} phosphor.[25] It should be noted that the PL spectra of Eu^{2+}(I) and Eu^{2+}(II) can be obtained as follows: Upon different excitation wavelength, the different shape of the PL spectra can be obtained, since these PL spectra are all composed of Eu^{2+}(I) and Eu^{2+}(II). After simple subtraction, we can finally obtain the individual PL spectra of Eu^{2+}(I) and Eu^{2+}(II).

3.2. Luminescence Properties and Energy Transfer in BMAS: Eu^{2+}, Tb^{3+}. The PL and PLE spectra of the Eu^{2+} and Tb^{3+} singly doped BMAS phosphors are shown in Figure 3a and b. The PLE spectrum of Tb^{3+} consists of several lines in the region from 300 to 500 nm, which corresponds to absorption f−f transition of the Tb^{3+} ion.[26] The Tb^{3+} emission lines are located at 485, 545, 580, and 620 nm, which are assigned to the $^5D_4$−^7F_J = (J = 6, 5, 4, 3) multiplet transitions, respectively. Compared to the PL spectrum of BMAS: Eu^{2+} (Figure 3a), BMAS: Tb^{3+} shows very weak emission upon near UV light excitation due to forbidden f−f absorption transitions of Tb^{3+} in UV. It is clearly exhibited that there is a significant spectral overlap between the Eu^{2+} PL and Tb^{3+} PLE spectra, indicating the possibility of energy transfer from Eu^{2+} to Tb^{3+} in BMAS. Figure 3c illustrates the PLE and PL spectra of BMAS: 0.04Eu^{2+}, 0.1Tb^{3+}. It is observed that the PLE spectrum monitoring the 542 nm emission of the Tb^{3+} is similar to that monitoring the blue emission (450 nm) of Eu^{2+}(II) and different from that of Eu^{2+}(I) (see Figure 2), demonstrating the existence of energy transfer from Eu^{2+}(II) to Tb^{3+} in BMAS systems. While, the emission intensity of Tb^{3+} is considerably enhanced to compare the Eu^{2+} emission due to energy transfer from Eu^{2+}(II) to Tb^{3+}.

A series of the emission spectra for BMAS: 0.04Eu^{2+}, yTb^{3+} (y = 0, 0.02, 0.04, 0.06, 0.08, and 0.1) under UV excitation (λ_{ex} = 330 nm) are carried out as shown in Figure 4. With increasing Tb^{3+} concentration, the emission intensities of the Tb^{3+} increase followed by the decrease of Eu^{2+} emission intensities, reflecting the result of energy transfer from Eu^{2+} to Tb^{3+}.

To further understand the process of energy transfer, the fluorescence lifetimes τ_1 for Eu^{2+}(I) and τ_2 for Eu^{2+}(II) with

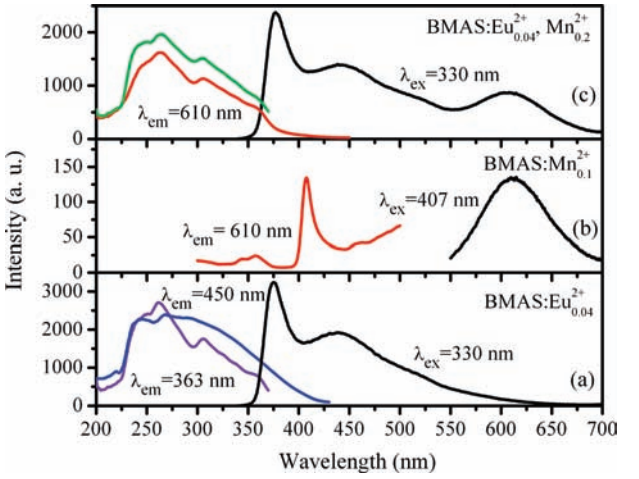

Figure 6. The excitation and emission spectra of BMAS: Eu^{2+}(a), BMAS: Mn^{2+} (b), and BMAS: Eu^{2+}, Mn^{2+}(c) phosphors.

different Tb^{3+} concentrations are measured and presented in Figure 5. The values of the lifetimes are obtained by integrating the decay curves of which the initial intensities are normalized. With increasing Tb^{3+} concentration, the values of τ_2 gradually decreases, however that of τ_1 exhibits no significant change. This behavior further indicates that the energy transfer is dominated by Eu^{2+}(II)−Tb^{3+} transfer rather than by Eu^{2+}(I)−Tb^{3+} transfer. The energy-transfer efficiency η_{Eu-Tb} can be calculated using

$$\eta_{Eu-Tb} = 1 - \tau_2/\tau_{20} \quad (1)$$

where τ_{20} is the lifetimes for Eu^{2+}(II) in the absence of Tb^{3+}. The calculated energy-transfer efficiency is shown in Figure 5. With increasing Tb^{3+} concentration, η_{Eu-Tb} increases and reaches 11% at y = 0.1. Although the efficiency is not high enough, the PL spectra in Figure 4 still demonstrate strong emissions of Tb^{3+} to enrich the green-emitting color of the phosphors for potential use in white LED and FLs.

3.3. Luminescence Properties and Energy Transfer in BMAS: Eu^{2+}, Mn^{2+}. The PL and PLE spectra of the Eu^{2+} and Mn^{2+} singly doped BMAS phosphors are shown in Figure 6a and b. BMAS: Mn^{2+} phosphor exhibits a weak red emission band

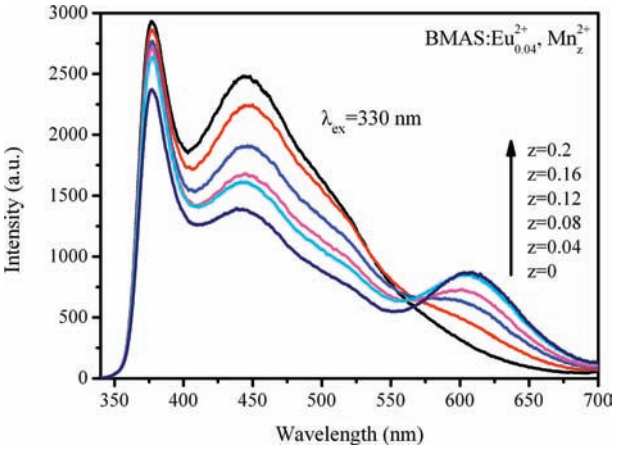

Figure 7. The PL spectra of BMAS:0.04Eu^{2+}, zMn^{2+} phosphors with different doping contents z at the excitation wavelength of 330 nm.

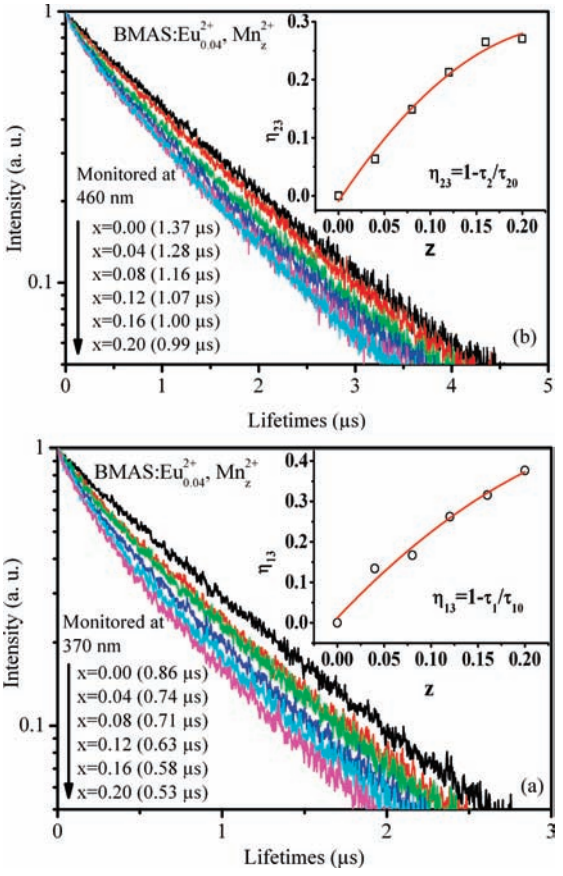

Figure 8. The fluorescence lifetimes of Eu^{2+}(I) (τ_1) (a), Eu^{2+}(I) (τ_2) (b) in BMAS: 0.04Eu^{2+}, zMn^{2+} (z = 0, 0.04, 0.08, 0.12, 0.16, and 0.2). Inset: The energy-transfer efficiency (η_{Eu-Mn}) with different doping Mn^{2+} contents.

peaking at 610 nm originating from $^4T_1-^6A_1$ transition of Mn^{2+} with its PLE peaks at 355 and 406 nm, corresponding to the forbidden transitions from the ground state $^6A_1(6_S)$ to $^4T_2(^4D)$ and ($^4A_1(^4G)$, $^4E(^4G)$) levels of Mn^{2+}, respectively.[27] Figure 6c shows the PLE and PL spectra of BMAS: 0.04Eu^{2+}, 0.2Mn^{2+}. The green solid line exhibits a combined PLE spectrum of Eu^{2+}(I) and Eu^{2+}(II) with the intensity ratio of 1.2 for Eu^{2+}(II) to Eu^{2+}(I) at the wavelength of 330 nm. This ratio is originated from

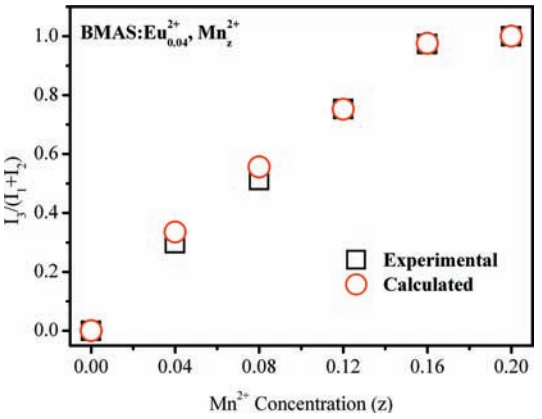

Figure 9. Calculated and experimental ratios of $I_3/(I_2 + I_1)$ intensity ratios at various Mn^{2+} concentrations. The ratios are scaled to the maximum.

eq 3. It is noticed that, different from BMAS: 0.04Eu^{2+}, 0.1Tb^{3+}, the PLE spectrum monitoring the red emission of the Mn^{2+} is similar to the combined PLE spectrum of Eu^{2+}(I) and Eu^{2+}(II) (green solid line), indicating the energy transfer occurred from both Eu^{2+}(I) and Eu^{2+}(II) to Mn^{2+}.

Figure 7 shows the PL spectra of BMAS:0.04Eu^{2+}, zMn^{2+} phosphors with different Mn^{2+} concentrations (z = 0, 0.04, 0.08, 0.12, 0.16, and 0.20) under 330 nm excitation. With increasing z, the emission intensity of Mn^{2+} ions increases followed by emission decreases of Eu^{2+} due to Eu^{2+}−Mn^{2+} energy transfer.

The decay curves of Eu^{2+}(I) and Eu^{2+}(II) fluorescence in BMAS: 0.04Eu^{2+}, zMn^{2+} (z = 0, 0.04, 0.08, 0.12, 0.16, and 0.2) are measured and shown in Figure 8. The reduction of the lifetimes for Eu^{2+} with increasing Mn^{2+} concentrations is observed. These results support the efficient energy transfer from Eu^{2+} to Mn^{2+}.

The energy-transfer processes can be described as follows: the three emitting centers at 376, 450, and 610 nm are labeled by 1, 2, and 3, respectively, and the energy transfer from their center is considered. The energy-transfer efficiency can be obtained using the eq 1, as shown in Figure 8a and b inset. It can be seen that the values of η_{13} and η_{23} gradually increase and reach to 38% of Eu^{2+}(I) and 27% of Eu^{2+}(II) for Mn^{2+} concentrations at z = 0.2, further implying the energy of the red emission of Mn^{2+} is derived from both Eu^{2+}(I) and Eu^{2+}(II). In continuous excitation, the number of Eu^{2+} excited-state rate equation for center 1 and 2 with 3 has the relationship as

$$W_{13}n_1 + W_{23}n_2 = n_3/\tau_3 \quad (2)$$

where n_i and W_{i3} are population of center i and energy-transfer rate from center i to 3, respectively, and τ_3 is fluorescence lifetimes of Mn^{2+}. If the emission intensity and the radiative transition rate of center i are denoted by I_i and γ_i, the intensity ratio of the red emission of Mn^{2+} to the emission of Eu^{2+} is determined by the following equation:

$$\frac{I_3}{I_1 + I_2} = \tau_3\gamma_3\left(\frac{W_{13}I_1}{\gamma_1(I_1 + I_2)} + \frac{W_{23}I_2}{\gamma_2(I_1 + I_2)}\right) \quad (3)$$

where $W_{13} = 1/\tau_1 - 1/\tau_{10}$, $W_{23} = 1/\tau_2 - 1/\tau_{20}$, and τ_{10} and τ_{20} are the fluorescence lifetimes of Eu^{2+}(I) and Eu^{2+}(II) in the absence of Mn^{2+}, respectively. The $I_3/(I_2 + I_1)$ integral intensity ratio of the Mn^{2+} emission to the Eu^{2+} emission can be calculated according to the emission spectra in Figure 7. The γ_1 and γ_2 are obtained from intrinsic lifetime measurements of 376 and

dx.doi.org/10.1021/ic201033e |Inorg. Chem. 2011, 50, 7846–7851

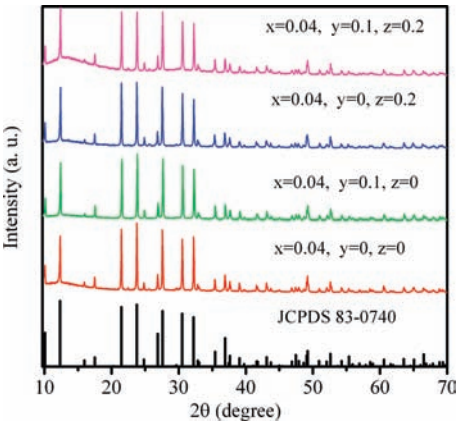

Figure 10. XRD patterns of BMAS:Eu^{2+}, Tb^{3+}, Mn^{2+} with varying Tb^{3+} and Mn^{2+} concentrations.

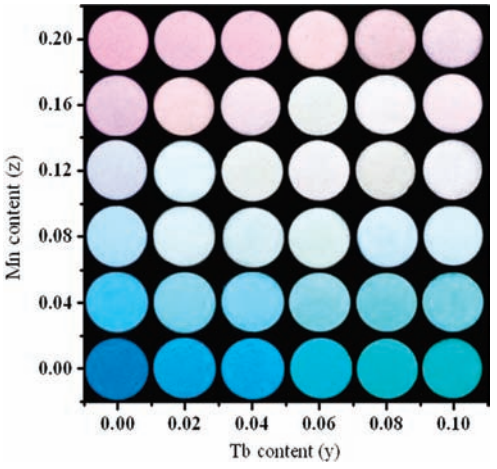

Figure 11. The photographs of the emission BMAS:0.04Eu^{2+}, yTb^{3+}, zMn^{2+} phosphors with different percent of dopant contents (y and z) under excitation at 365 nm.

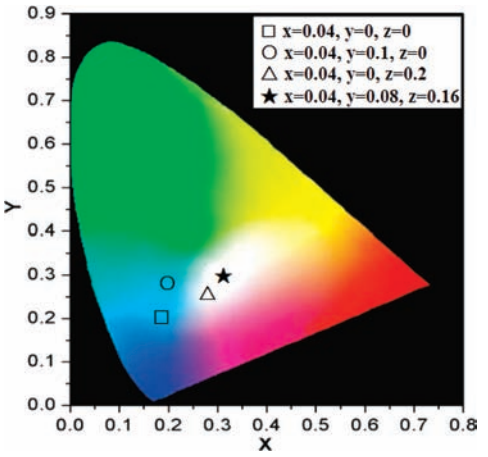

Figure 12. CIE chromaticity diagram of BMAS:0.04Eu^{2+}, yTb^{3+}, zMn^{2+} phosphors under 365 nm excitation.

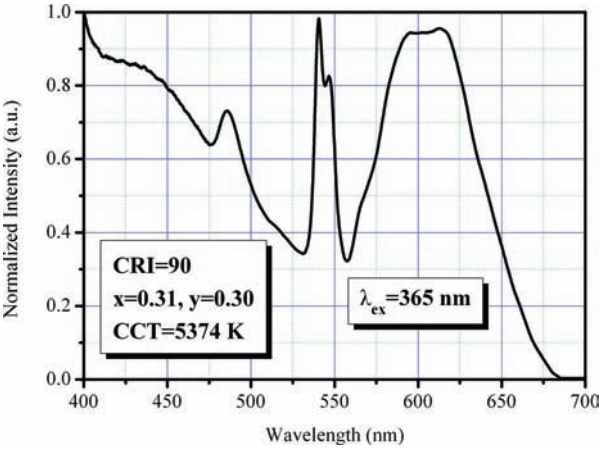

Figure 13. The PL spectra of a single composition BMAS: 0.04Eu^{2+}, 0.08Tb^{3+}, 0.16Mn^{2+} phosphor under 365 nm excitation.

450 nm emissions, respectively, in BMAS: 0.005Eu^{2+} to avoid concentration and nonradiative transition effects, and τ_3 has been measured and nearly unchanged for different Mn^{2+} concentrations. At each fixed concentration, the energy of Mn^{2+}can be estimated using eq 3 from the contribution of Eu^{2+}(I) and Eu^{2+}(II) (first and the second terms in eq 3), it is found that the contribution of Eu^{2+}(II) is 1.2 times larger than that of Eu^{2+}(I) for BMAS: 0.04Eu^{2+}, 0.2Mn^{2+}sample, supporting our fitted excitation spectrum in Figure 6c. The $I_3/(I_2 + I_1)$ intensity ratios at various Mn^{2+} concentrations are calculated using eq 3 and scaled to the maximum, as presented in Figure 9. For comparison, the intensity ratios obtained directly from the emission spectra are also given in Figure 9. It can be seen that the calculated data are in good agreement with the experimental ones, clearly demonstrating the correction of our above luminescence dynamical analysis, as described in eq 3.

3.4. Luminescence, Chromaticity, and Thermal Stability Study of BMAS:Eu^{2+}, Tb^{3+}, Mn^{2+}. XRD patterns of BMAS: Eu^{2+}, Tb^{3+}, Mn^{2+} with various Tb^{3+} and Mn^{2+} concentrations are shown in Figure 10. The XRD patterns of all phosphors are identical to JCPDS 83−0740 of the BMAS host structure.

According to our study above, it is not observed that there exists a spectral overlap between Tb^{3+} PL and Mn^{2+} PLE or Mn^{2+} PL and Tb^{3+} PLE spectra. Thus, there could not be any energy transfer between Tb^{3+} and Mn^{2+} in BMAS: Eu^{2+}, Tb^{3+}, Mn^{2+} samples. Our white-emitting BMAS:Eu^{2+}, Tb^{3+}, Mn^{2+}phosphors are still based on energy transfer from $Eu^{2+}$to Tb^{3+} and Eu^{2+} to Mn^{2+}, respectively. Figure 11 displays the photographs of the emitting phosphors BMAS:0.04Eu^{2+}, yTb^{3+}, zMn^{2+} with different compositional concentrations (y and z) under excitation at 365 nm. By varying y and z, the emitting color is able to be tuned from blue to green or red, which demonstrates controllable emitting colors as a function of Tb^{3+} and Mn^{2+} contents. The emitting color points including a white light point selected samples are illustrated in the Commission on Illumination (CIE) chromaticity diagram, as shown in Figure 12. Figure 13 shows PL spectra of white light-emitting BMAS: 0.04Eu^{2+}, 0.08Tb^{3+}, 0.16Mn^{2+} phosphor in the visible range upon 365 nm excitation. The corresponding CIE color coordinates and correlated color temperature of the phosphor are (0.31, 0.30) and 5374 K, respectively. The CRI (R_a) is significantly as high as 90, observed to be higher than that ($R_a \approx 78$) of a LED based on YAG:Ce with blue InGaN chip and that ($R_a \approx 85$) of FLs based on triphosphors. Our results indicate that BMAS:Eu^{2+}, Tb^{3+}, Mn^{2+} is a great potential and flexible candidate for using single phosphor converted white light sources, such as UV LED-based white LED and present FLs.

dx.doi.org/10.1021/ic201033e |Inorg. Chem. 2011, 50, 7846–7851

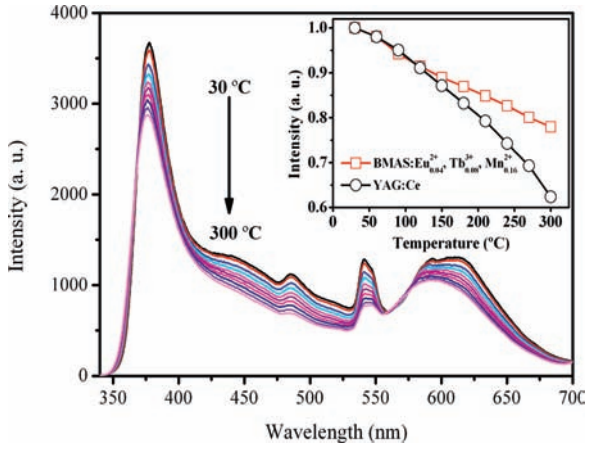

Figure 14. The temperature-dependent emission intensity of the optimized BMAS:0.04Eu^{2+}, 0.08Tb^{3+}, 0.16Mn^{2+} sample.

In the white LED application, a low-temperature quenching effect is in favor of keeping the chromaticity and the brightness of white light output. The temperature-dependent emission intensity of the optimized BMAS:0.04Eu^{2+}, 0.08Tb^{3+}, 0.16Mn^{2+} sample is shown in Figure 14. As the temperature rises from 30 to 150 °C at which the white LEDs usually work, the emission intensity of BMAS:0.04Eu^{2+}, 0.08Tb^{3+}, 0.16Mn^{2+} remains at about 88% of that measured at room temperature, while at about 86% for the YAG:Ce^{3+} phosphor (Figure 14 inset), indicating the phosphor is as good as YAG:Ce in terms of their thermal quenching properties, and beyond 150 °C, the BMAS:0.04Eu^{2+}, 0.08Tb^{3+}, 0.16Mn^{2+} sample is even better.

4. CONCLUSION

In summary, we have synthesized a series of novel emission-tunable $BaMg_2Al_6Si_9O_{30}$:Eu^{2+}, Tb^{3+}, Mn^{2+} phosphors by a solid-state reaction. The obtained phosphor exhibits a broad excitation band ranging from 200 to 400 nm, which can perfectly match UV excitation light. The $BaMg_2Al_6Si_9O_{30}$:Eu^{2+}, Tb^{3+}, Mn^{2+} phosphors show three emission colors: blue band of 450 nm, green band of 542 nm and red band of 610 nm. The energy transfer from Eu^{2+} to Tb^{3+} and Eu^{2+} to Mn^{2+}in $BaMg_2Al_6Si_9O_{30}$ host matrix is demonstrated by luminescence spectra, energy-transfer efficiency, and lifetimes of phosphors. Furthermore, the energy transfer leads to the following results: (1) The energy transfer of Eu^{2+}—Tb^{3+} is dominated by Eu^{2+}(II)—Tb^{3+} transfer rather than Eu^{2+}(I)—Tb^{3+} transfer; (2) the energy of the red emission of Mn^{2+} is considered to come from both Eu^{2+}(I) and Eu^{2+}(II); and (3) the ratio of the red emission of Mn^{2+} to the emission of Eu^{2+} by experiment is consistent with the theoretical calculation based on energy-transfer and lifetime measurements. We have demonstrated that the varied emitted color from blue to green or red and eventually to white can be achieved by properly tuning the relative ratio of Tb^{3+} and Mn^{2+}. All these results indicate that $BaMg_2Al_6Si_9O_{30}$:Eu^{2+}, Tb^{3+}, Mn^{2+} is a promising single-composition phosphor for applications involving white light LED and FLs lamps.

AUTHOR INFORMATION

Corresponding Author

*E-mail: zhangjh@ciomp.ac.cn; Telephone/Fax: +86-431-8617-6317.

ACKNOWLEDGMENT

This work is financially supported by the National Nature Science Foundation of China (10834006, 10904141, 10904140), the MOST of china (2010AA03A404) and the Scientific project of Jilin province (20090134, 20090524) and CAS Innovation Program.

REFERENCES

(1) Nakamura, S.; Fasol, G. *The Blue Laser Diode*; Springer: Berlin, Germany, 1996.
(2) Nakamura, S. *MRS Bull.* **2009**, *34*, 101.
(3) Setlur, A. A.; Heward, W. J.; Gao, Y.; Srivastava, A. M.; Chandran, R. G.; Shankar, M. V. *Chem. Mater.* **2006**, *18*, 3314.
(4) Batentschuk, M.; Osvet, A.; Schierning, G.; Klier, A.; Schneider, J.; Winnacker, A. *Radiat. Meas.* **2004**, *38*, 539.
(5) Jang, H. S.; Won, Y. H.; Jeon, D. Y. *Appl. Phys. B: Lasers Opt.* **2009**, *95*, 715.
(6) Hao, Z. D.; Zhang, J. H.; Zhang, X.; Sun, X. Y.; Luo, Y. S.; Lu, S. Z.; Wang, X. J. *Appl. Phys. Lett.* **2007**, *90* (26), 261113.
(7) Kim, J. S.; Jeon, P. E.; Park, Y. H.; Choi, J. C.; Park, H. L.; Kim, G. C.; Kim, T. W. *Appl. Phys. Lett.* **2004**, *85* (17), 3696.
(8) Yang, W. J.; Chen, T. M. *Appl. Phys. Lett.* **2007**, *90* (17), 171908.
(9) Kido, J.; Shionoya, H.; Nagai, K. *Appl. Phys. Lett.* **1995**, *67*, 2281.
(10) Piao, X. Q.; Horikawa, T.; Hanzawa, H.; Machida, K. *Appl. Phys. Lett.* **2006**, *88*, 161908.
(11) Huang, C. H.; Chen, T. M. *Opt. Express* **2010**, *18*, 5089.
(12) Huang, C. H.; Chen, T. M.; Liu, W. R.; Chiu, Y. C.; Yeh, Y. T.; Jang, S. M. *ACS Appl. Mater. Interfaces* **2010**, *2*, 259.
(13) Guo, N.; Huang, Y. J.; You, H. P.; Yang, M.; Song, Y. H.; Liu, K.; Zheng, Y. H. *Inorg. Chem.* **2010**, *49* (23), 10907.
(14) Huang, C. H.; Liu, W. R.; Chen, T. M. *J. Phys. Chem. C* **2010**, *114*, 18698.
(15) Guo, N.; You, H. P.; Song, Y. H.; Yang, M.; Liu, K.; Zheng, Y. H.; Huang, Y. J.; Zhang, H. J. *J. Mater. Chem.* **2010**, *20*, 9061.
(16) Guo, C. F.; Yu, J.; Ding, X.; Li, M.; Ren, Z. Y.; Bai, J. T. *J. Electrochem. Soc.* **2011**, *158* (2), J42.
(17) Huang, C. H.; Kuo, T. W.; Chen, T. M. *ACS Appl. Mater. Interfaces* **2010**, *2*, 1395.
(18) Huang, C. H.; Chen, T. M. *J. Phys. Chem. C* **2011**, *115* (5), 2349.
(19) Zhang, G. G.; Wang, J.; Chen, Y.; Su, Q. *Opt. Lett.* **2010**, *35*, 2382.
(20) Jiao, H. Y.; Wang, Y. H. *J. Electrochem. Soc.* **2009**, *156* (5), J117.
(21) Kim, J. S.; Kim, G. C.; Kim, T. W. *Appl. Phys. Lett.* **2004**, *85*, 3696.
(22) Rao, R. P. *J. Electrochem. Soc.* **2003**, *150*, H165.
(23) Larson, A. C.; Von Dreele, R. B. *Los Alamos Natl. Lab., [Rep.] LA (U. S.)* **1994**, *86*, 748.
(24) Wolfgang, W.; Armbruster, T.; Lengauer, C. *Eur. J. Mineral.* **1995**, *7*, 277.
(25) Im, W. B.; Kim, Y, I.; Jeon, D. Y. *Chem. Mater.* **2006**, *18*, 1190.
(26) Li, Y. C.; Chang, Y. S.; Lai, Y. C.; Lin, Y. J.; Laing, C. H.; Chang, Y. H. *Mater. Sci. Eng., B* **2008**, *146*, 225.
(27) Yang, W. J.; Luo, L. Y.; Chen, T. M.; Wang, N. S. *Chem. Mater.* **2005**, *17*, 3883.